033256-1-T

A HYBRID FINITE ELEMENT-FAST MULTIPOLE TECHNIQUE FOR ELECTROMAGNETIC SCATTERING

S.S. Bindiganavale and J.L. Volakis

Naval Air Warfare Center Weapons Div.
China Lake, CA 93555-6001

January 1996

33256-2-T = RL-2456

Report #033762-1-T

Contract Title:	Further development of FEMATS including prismatic meshes, graphical interface and new mesh truncation schemes
Contract No.:	N68936-95-C-0349
Report Title:	A hybrid FEM-FMM technique for electromagnetic scattering
Report Authors:	Sunil S. Bindiganavale and John L. Volakis
Primary University Collaborator:	John L. Volakis
Contract monitor:	Dr. Helen Wang Code 455520D Bldg 31567 Naval Air Warfare Center Weapons Division China Lake, CA 93555
University Address:	Radiation Laboratory Department of Electrical Engineering and Computer Science Ann Arbor, MI 48109–2122 Email: volakis@umich.edu Phone: (313)764-0500
Date:	January 1996

A hybrid FEM-FMM technique for electromagnetic scattering

Sunil S. Bindiganavale and John L. Volakis

Radiation Laboratory
Department of Electrical Engineering and Computer Science
The University of Michigan
Ann Arbor, MI 48109-2122

Abstract

In this paper, we apply a version of the Fast Multipole Method (FMM) to reduce the storage and computational requirement of the boundary integral in the finite element-boundary integral method. By virtue of its $0(N^{1.5})$ operation count, the application of the single-stage FMM, results in substantial speed-up of the boundary integral portion of the code, independent of the shape of the BI contour. We will discuss the efficiency of the method and present the application of this technique to the computation of electromagnetic scattering from large grooves recessed in a ground plane.

1 Introduction

Over the past few years different hybrid versions of the finite element method have been explored for application to scattering by composite structures. Among them, the finite element-boundary integral equation (FE-BI) and the finite element-absorber boundary condition (FE-ABC) methods have been quite popular and extensively applied to many applications. The FE-BI method [1],[2] employs the exact boundary integral equation which provides

an independent relation between the tangential E and H fields on the mesh outer boundary and is therefore an exact method. This is in contrast to the FE-ABC method [3] which employs an approximate truncation operator but leads to fully sparse systems. On the other hand, the FE-BI method, although "exact", leads to a partly full and partly sparse system (see figure 1) and is thus more computationally intensive. For special cases, where the boundary is rectangular or circular, the FFT can be used [4] to reduce the memory and CPU requirements to $N \log N$. However, in general, the boundary integral is not convolutional and in that case the CPU requirements will be of $O(N_b^2)$ where N_b denotes the unknowns on the boundary.

In this paper, we apply a version of the Fast Multipole Method (FMM) to reduce the storage and computational requirement of the boundary integral when the size of the contour is large. By virtue of its $0(N^{1.5})$ operation count, the application of the FMM, results in substantial speed-up of the boundary integral portion of the code, independent of the shape of the BI contour. We consider the application of this technique (referred to hereon as the FEM-FMM method) to scattering from a material-filled groove in a conducting plane. The FEM is employed to formulate the fields within the cavity and establish a relationship with those at the aperture. The fields external to the groove are expressed as an integral over the aperture and a system of integral equations is then obtained by enforcing field continuity across the aperture. To reduce the storage requirement and speed up the computation of the boundary integral, an approximate version of the fast multipole method [5] is employed.

2 Formulation

Consider a filled PEC groove of width w and depth d in an otherwise uniform ground plane as shown in figure 2(a). The material filling the groove has a permittivity ϵ_r and permeability μ_r. The free space region exterior to the groove is denoted as region I while the groove itself is denoted as region II (see figure 2). The fields in the two regions are decoupled by closing the aperture with a perfect conductor and introducing an equivalent magnetic current based on the equivalence principle

$$\mathbf{M}_1 = \mathbf{E}_1 \times \hat{y} \tag{1}$$

where $\mathbf{E}_1$ is the electric field at the aperture. The ground plane can be removed by application of image theory and hence the field in region I can be expressed as the radiation caused by $\mathbf{M}_1$ and the external sources $(\mathbf{J}^i, \mathbf{M}^i)$. The coupling of the fields in each region is achieved by requiring continuity of the tangential magnetic field across the aperture

$$\mathbf{H}^I_{tan}|_{y=0} = \mathbf{H}^{II}_{tan}|_{y=0} \tag{2}$$

The magnetic field, $\mathbf{H}^{II}$, inside the groove is formulated via the finite element method which has the inherent geometrical and material adaptability and low $O(N)$ storage requirement. This procedure and the coupling in (2) is described in detail in [1]. $\mathbf{H}^I$ is expressed as an integral of $\mathbf{M}_1$ using the free space Green's function. To this integral equation we apply a version of the fast multipole method [5] to reduce the operation count from $O(N_b^2)$ to $O(N_b^{1.5})$ where N_b is the number of unknowns on the boundary; the next section describes this procedure for TE incidence.

2.1 Boundary integral for TE case

The groove is illuminated by the plane wave

$$\mathbf{H}^i = \hat{z} e^{jk_0(x\sin\phi_0 + y\cos\phi_0)} \tag{3}$$

where $k_0 = 2\pi/\lambda_0$ is the free space wavenumber and ϕ_0 is the angle of incidence. With a z-directed impressed magnetic field $\mathbf{H}^i$, the scattered magnetic field will also be z-directed, and consequently the equivalent magnetic current $\mathbf{M}_1$ may be written as

$$\mathbf{M}_1 = \hat{z} M_1(x) \tag{4}$$

From figure 2(b), the magnetic field in region I due to M_1 is given by

$$\begin{aligned} H^I_z(\mathbf{r}) &= H^{inc}_z(x,y) + H^{refl}_z(x,y) \\ &- jk_0 Y_0 \int_{C_1} M_1(x') G_0(\rho,\rho') dx' \end{aligned} \tag{5}$$

where

$$G_0(\rho,\rho') = \frac{-j}{2}\left\{ H_0^{(2)}\left(k_0\sqrt{(x-x')^2 + (y-y')^2} \right) \right\} \tag{6}$$

is the free space Green's function. Applying Galerkin's technique to (5) yields the matrix equation

$$[C]\{\phi\} \;=\; \{\phi^{inc}\} - [P]\{\psi\} \tag{7}$$

where $\{\phi\}$ is the column vector with $N_b + 1$ elements representing the nodal magnetic field on C_1, and N_b is the number of segments employed for the discretization of C_1. $\{\psi\}$ is the column vector with N_b elements representing the magnetic current on the boundary. The column vector $\{\phi^{inc}\}$ has N_b elements given by

$$\phi_m^{inc} = \left(H_z^{inc}(x_m, 0) + H_z^{refl}(x_m, 0)\right) \Delta x_m, \quad m = 1, 2, \ldots, N_b \tag{8}$$

with Δx_m being the segment length of the mth segment on C_1 and x_m being its midpoint. The product $[C]\{\phi\}$ in (7) is of not much concern since $[C]$ is a sparse matrix assembled from the interaction of the magnetic field and current on the boundary segments. The product $[P]\{\psi\}$ is of concern because of the $0(N_b^2)$ storage required by the full matrix $[P]$ whose elements are given by

$$P_{mn} \;=\; \frac{-j}{2}\left\{H_0^{(2)}\left(k_0\left|x_m - x_n\right|\right)\Delta x_m \Delta x_n\right\} \quad m \neq n \tag{9}$$

To employ the approximate version of the FMM in solving (7), the unknowns on the boundary are divided into groups with M_b unknowns in each group and thus the number of groups will then be $\frac{N_b}{M_b}$. For large source to observation distances, the kernel in (9) is approximated by using the large argument expansion as [5]

$$H_0^{(2)}(k_0\left|x_m - x_n\right|) \sim e^{-\mathrm{j}k_0 x_{lm}} \sqrt{\frac{2\mathrm{j}}{\pi}} \frac{e^{-\mathrm{j}k_0 x_{l'l}}}{\sqrt{k_0 x_{l'l}}} e^{-\mathrm{j}k_0 x_{nl'}} \tag{10}$$

where $x_{l'l}$ is the distance between the center of the test group l and the center of the source group l'; $x_{nl'}$ is the distance between the nth source element and its group center and x_{lm} is the distance between the mth test element and its group center. The decoupling of test-source element interactions in the kernel as in (10) enables the computation of the matrix-vector product for far-field groups with a reduced operation count as detailed in the following sequence.

1. For each test group, the aggregation of source elements in a single source group involves M_b operations, corresponding to the number of elements in the source group. The aggregation operation corresponds to

$$b_{l'l} = \sum_{j=1}^{M_b} M_j e^{-\mathrm{j}k_0 x_{nl'}} \tag{11}$$

2. Since the above aggregation operation needs to be done for all source groups the operation count becomes $O(\frac{N_b}{M_b} M_b) \sim O(N_b)$, where $\frac{N_b}{M_b}$ represents the total number of groups. Also this operation, being dependent only on the test *group* rather than the test *element*, needs to be repeated for $\frac{N_b}{M_b}$ test groups leading to a total operation count of $O(\frac{N_b^2}{M_b})$ for aggregation.

3. The next step would be a translation operation corresponding to

$$c_{l'l} = \sqrt{\frac{2\mathrm{j}}{\pi}} \frac{e^{-\mathrm{j}k_0 x_{l'l}}}{\sqrt{k_0 x_{l'l}}} b_{l'l} \tag{12}$$

   Since this needs to be done only at the group level, it involves $O(\frac{N_b^2}{M_b^2})$ operations for all possible test and source group combinations and is the least computationally intensive step.

4. The final step in the sequence would be the process of disaggregation corresponding to the operation

$$I_{lm} = \sum_{l'=1}^{N_b/M_b} c_{l'l} e^{-\mathrm{j}k_0 x_{lm}} \tag{13}$$

   Conceptually, this process is the converse of aggregation. Since this operation involves only the source *group* instead of the source *element* it needs to be done for each source group thus implying an $O(\frac{N_b}{M_b})$ operation to generate a single row of the matrix-vector product. To generate M_b rows corresponding to a test group the operation count would be $O(N_b)$. With $\frac{N_b}{M_b}$ test groups, the operation count would be of $O(\frac{N_b^2}{M_b})$.

5. The near field operation count being of $O(N_b M_b)$ and the far field being $O(\frac{N_b^2}{M_b})$ gives a total operation count of

$$Op.count \sim C_1 N_b M_b + C_2 \frac{N_b^2}{M_b} \tag{14}$$

Typically, we can set the elements in each group, $M_b = \sqrt{N_b}$ and as a result the total operation count is $O\sim N_b^{1.5}$.

Once the currents are computed in this manner, the far-fields are computed in th usual manner. Thus the maximum computational requirement in this hybrid algorithm is $O(N^{1.5})$ unlike the usual FE-BI which results in $O(N^2)$ if the boundary has N unknowns.

3 Results

A computer code based on the above formulation was implemented and executed on a HP 9000/750 workstation with a peak flop rate of 23.7 MFLOPS. The geometry considered was the rectangular groove shown in figure 1. Figure 3 shows the bistatic RCS at normal incidence for a groove 20λ wide and 0.25λ deep with a material filling of $\epsilon_r = 4$ and $\mu_r = 1$. The discretization of this geometry results in 2106 unknowns with a boundary integral of 300 unknowns. To obtain a measure of the speed-up realized by the application of the FEM-FMM to this problem, we refer to the CPU time comparisons also shown in figure 3. The compiled data on the FE-BI and FEM-FMM methods include the CPU time, storage requirement and average error. Data are also give for the FE-BI implementation using the special CG-FFT solver but it should be noted that the application of the CG-FFT is only suited for planar apertures. Clearly, the compiled run data show that the FEM-FMM is about three times faster than the traditional FE-BI implementation and requires only one sixth of the memory. However, the FEM-FMM has some deterioration in accuracy (average error of 2 dB for this example [6]) and this should be considered depending on the application and usage of the results. Similar data shown in figure 4 for plane wave incidence at an off-normal incidence angle (45^0) seem to verify the previous conclusions. The groove analyzed in figure 4 is 30λ wide and is 0.15λ deep with a material filling of $\epsilon_r = 6$ and $\mu_r = 1$. The discretization of this geometry results in 1803 unknowns with a

boundary integral of 450 unknowns. The error in the FEM-FMM solution is lower but this could be attributed to the use of a larger near-group window (4.3λ instead of 2.45λ) which results in an increase in storage and execution time of the boundary integral. Clearly the CG-FFT solver is substantially faster and arguably uncontested by the FEM-FMM method. This simply gives credence to modifications of the boundary integral surface so that the CG-FFT can be applied whenever possible even though the boundary surface may not be completely planar.

References

[1] J.M. Jin and J.L. Volakis, "TE scattering by an inhomogeneously filled aperture in a thick conducting plane," *IEEE Trans. Antennas Propagat.*, vol.38, pp.1280-1286, Aug. 1990.

[2] J.M. Jin and J.L. Volakis, "TM scattering by an inhomogeneously filled aperture in a thick conducting plane," *IEE Proc.*, pt. H, vol.137, pp. 153-159, June 1990.

[3] A. Chatterjee, J.M. Jin, and J.L. Volakis, "Edge-based finite elements and vector ABCs applied to 3D scattering," *IEEE Trans. Antennas Propagat.*, vol. 41, pp.221-226, Feb 1993.

[4] J.D. Collins, J.L. Volakis, and J.M. Jin, "A combined finite element-boundary element formulation for solution of two-dimensional scattering problems via CGFFT," *IEEE Trans. Antennas Propagat.*, vol. 38, pp. 1852-1858, 1990.

[5] C.C. Lu and W.C. Chew, Fast far field approximation for calculating the RCS of large objects, *Micro. Opt. Tech. Lett.*, 8(5):238-241, April 1995.

[6] S.S. Bindiganavale and J.L. Volakis, Guidelines for using the fast multipole method to calculate the RCS of large objects, *Micro. Opt. Tech. Lett.*, March 1996.

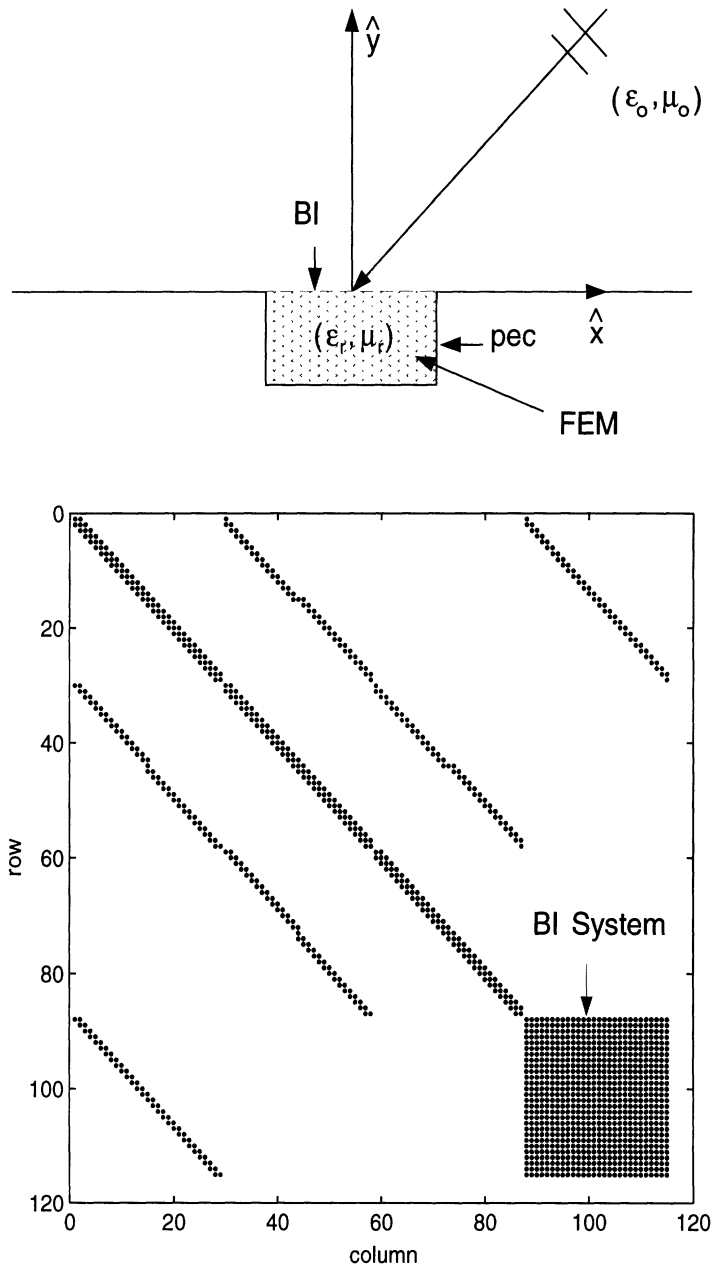

Figure 1: The FE-BI system matrix arising from the scattering/radiation problem of a groove in a ground plane. Unknowns 88-105 are the boundary integral unknowns.

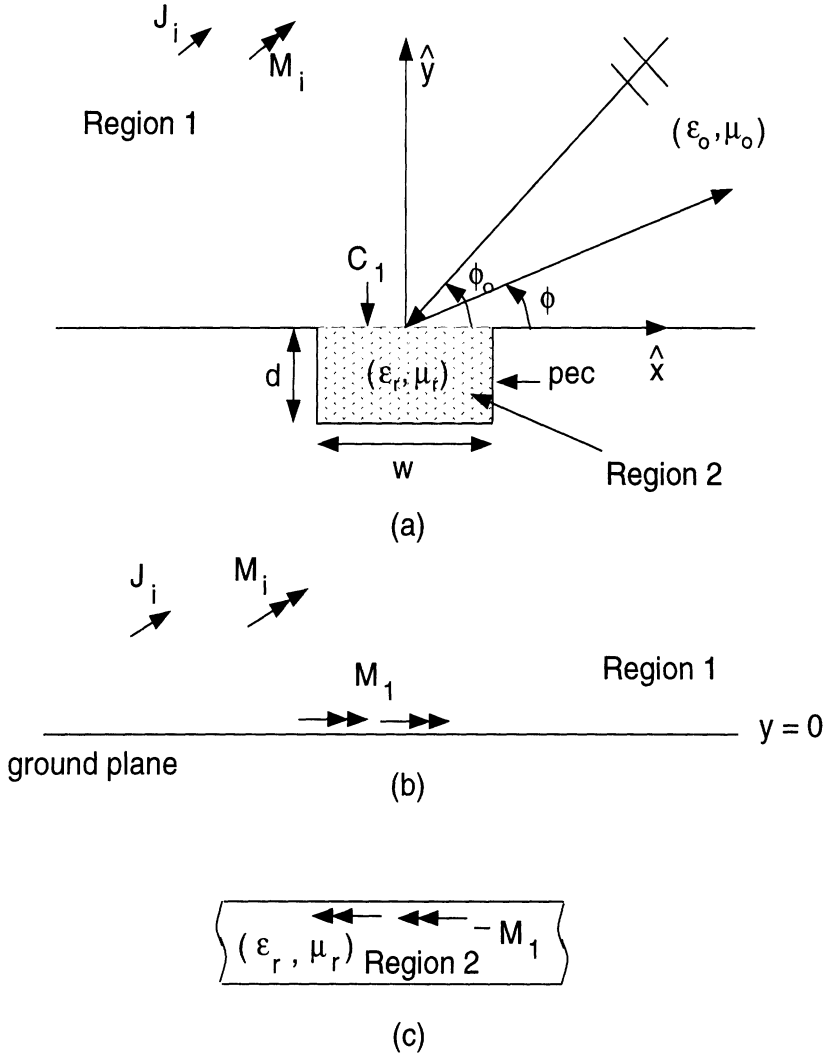

Figure 2: (a) Geometry of the groove recessed in a ground plane (b) Equivalent problem for region 1, and (c) region 2

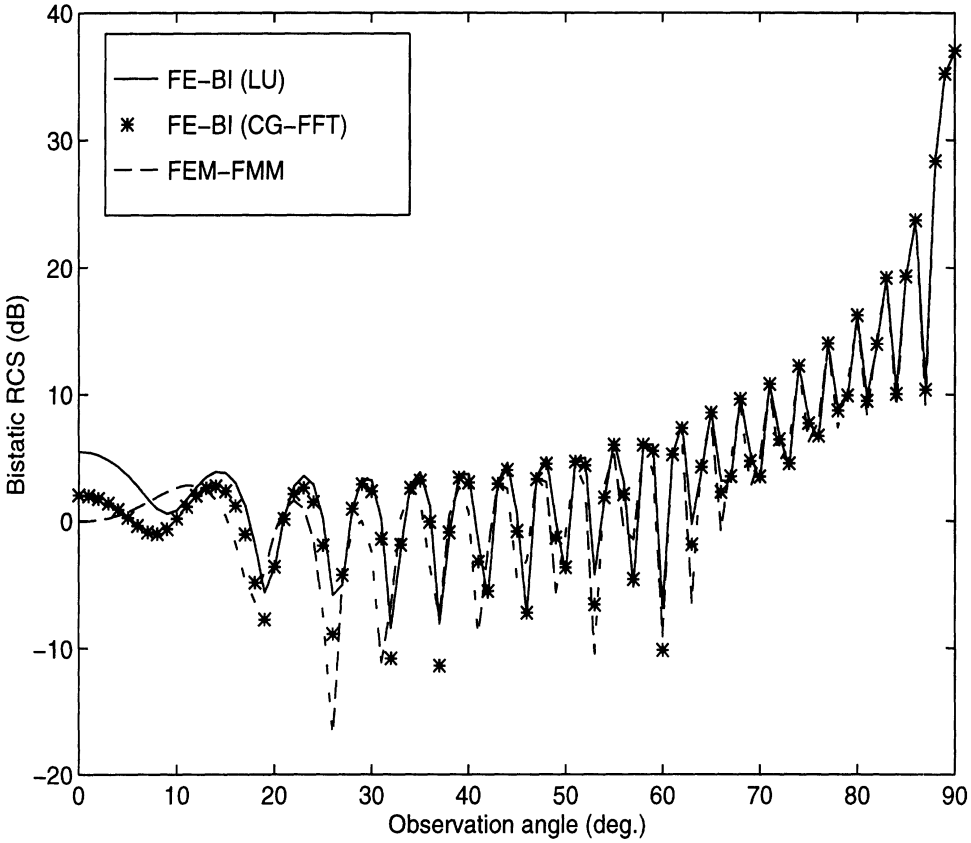

Time (for BI only)	FEM-BI (CG)	FEM-FMM	FEM-BI (CGFFT)
(Minutes,seconds)	15 mins 14 secs	4 mins 48 secs	1 min 40 secs

Memory (for BI only)	LU	FEM-FMM
(KB)	680	116

Average error	FEM-FMM	FEM-BI (CGFFT)
(dB)	2.016	0.98

Figure 3: Bistatic scattering from a rectangular groove 20λ wide and 0.35λ deep at normal incidence

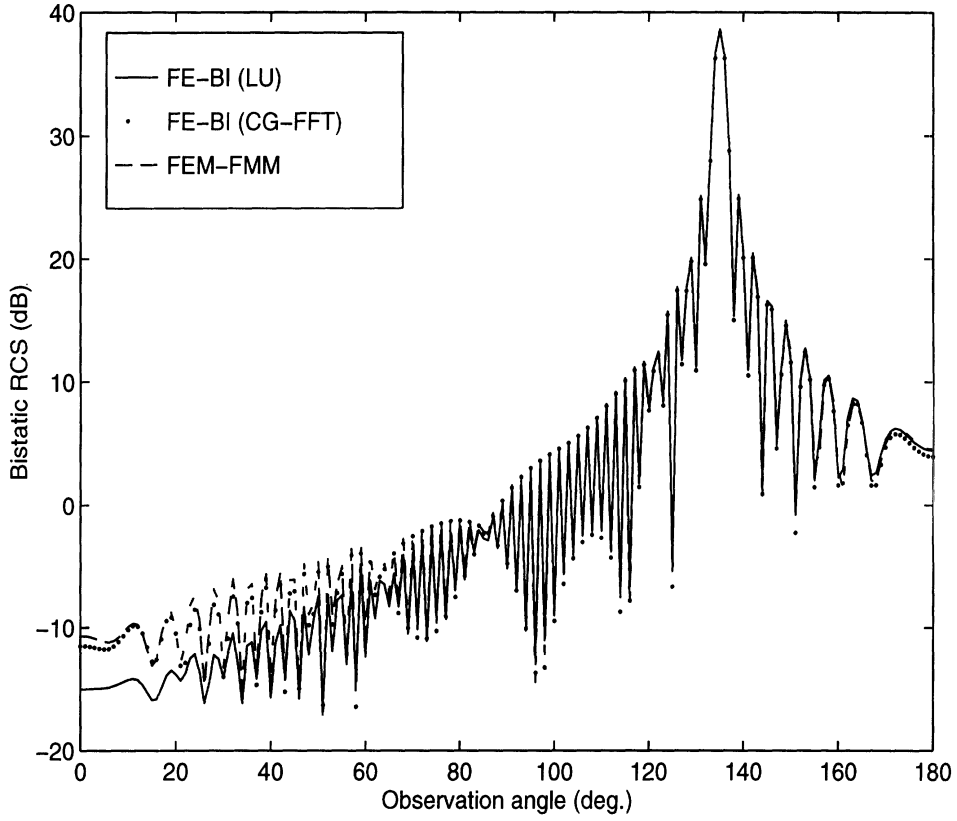

Time (for BI only)	FEM-BI (CG)	FEM-FMM	FEM-BI (CGFFT)
(Minutes,seconds)	30 mins 36 secs	9 mins 1 sec	2 min 15 secs

Memory (for BI only)	LU	FEM-FMM
(KB)	1544	436

Average error	FEM-FMM	FEM-BI (CGFFT)
(dB)	1.553	1.0267

Figure 4: Bistatic scattering from a rectangular groove 30λ wide and 0.15λ deep at 45^0 incidence